Available online at www.sciencedirect.com
ScienceDirect
Journal of Solid State Chemistry 180 (2007) 915–921
JOURNAL OF SOLID STATE CHEMISTRY
www.elsevier.com/locate/jssc

Defect structure of $Sb_{2-x}Fe_xTe_3$ single crystals

J. Horák[a], P. Lošťák[b], Č. Drašar[b,*], J. Navrátil[a], C. Uher[c]

[a]*Joint Laboratory of Solid State Chemistry, Institute of Macromolecular Chemistry of the Academy of Sciences of the Czech Republic, University of Pardubice, Studentská 84, 532 10 Pardubice, Czech Republic*
[b]*Faculty of Chemical Technology, University of Pardubice, Cs. Legii Square 565, 532 10 Pardubice, Czech Republic*
[c]*Department of Physics, University of Michigan, Ann Arbor, MI 48109-1120, USA*

Received 1 August 2006; received in revised form 14 December 2006; accepted 18 December 2006
Available online 28 December 2006

Abstract

Single crystals of $Sb_{2-x}Fe_xTe_3$ ($c_{Fe} = 0$–$9.5 \times 10^{19}\,cm^{-3}$) were prepared by Bridgman method. The interpretation of the reflection spectra in plasma resonance region indicates that Fe increases the concentration of holes (acceptor) and each Fe atom incorporated in Sb_2Te_3 structure liberates 0.4–0.5 hole. Observed effect is elucidated by means of point defect model. According to the model Fe atoms enter the structure and form uncharged substitutional defects $Fe^{\times}_{Sb}$. Since this defect cannot affect the free-carrier concentration directly, we assume an interaction of the entering Fe-atoms with natives defects leading to a rise in the concentration of antisite defects Sb'_{Te}, to a decrease of $V^{\bullet\bullet}_{Te}$ concentration, and to an increase in the concentration of holes.

Keywords: Antimony telluride; Defect structure; Optical properties

1. Introduction

Antimony telluride Sb_2Te_3 crystals belong to a family of layered semiconductors with the tetradymite structure (space group D^5_{3d}—$R\bar{3}m$). The trigonal lattice of Sb_2Te_3 is formed by a periodic arrangement of layers perpendicular to the trigonal axic c. Each layer is composed of five atomic planes arranged according to the following pattern:

$$\ldots Te^1 - Sb - Te^2 - Sb - Te^1 \ldots Te^1 - Sb - Te^2 - Sb - Te^1 \ldots .$$

Between Te^1 atomic planes of neighboring atoms there is a van der Waals gap [1]. This compound is a component of materials used in thermoelectric devices such as solid-state coolers and generators [2]. Therefore, an investigation of the effect of various dopants on the physical properties of Sb_2Te_3 is interesting both for basic and applied research.

Recently published studies on the influence of transition metals in the tetradymite-type crystals have revealed the existence of ferromagnetic ordering. These materials are thus classified as diluted magnetic semiconductors (DMS). The layered structure of the tetradymite-type matrix governs the distinct anisotropy of both the transport and magnetic properties. Incorporation of Fe atoms in Bi_2Te_3 led to low-temperature ferromagnetism [3,4]. A small content of vanadium in Sb_2Te_3 single crystals gave rise to ferromagnetic behavior at low temperatures; the Curie temperature increasing with vanadium concentration and reaching approximately 22 K for $Sb_{1.97}V_{0.03}Te_3$ [5,6]. Vanadium showed negligible effect on the concentration of holes. The Curie temperature of MBE-grown thin films of $Sb_{2-x}V_xTe_3$ reached 177 K [7]. According to the results of paper [8], Cr-doping in the Sb_2Te_3 crystals does not change the concentration of free current carriers, but their mobility decreases. Similar to the effect of vanadium, Cr induces ferromagnetic ordering up to 20 K [9]. Ferromagnetism of $Sb_{2-x}Cr_xTe_3$ is reported also in [10,11]. Although Mn is a typical stimulant of the magnetic order in intensively pursued III–V DMS, crystals of Mn-doped Sb_2Te_3 remain paramagnetic down to 2 K. The occurrence of high spin Mn^{2+} ions in $Sb_{2-x}Mn_xTe_3$ crystals gives rise to strong paramagnetism and the concentration of holes increases with the increasing content of incorporated Mn [12,13]. In contrast, the presence of titanium, zirconium or

*Corresponding author. Fax: +420 466 036 033.
E-mail address: cestmir.drasar@upce.cz (C. Drašar).

0022-4596/$ - see front matter © 2007 Elsevier Inc. All rights reserved.
doi:10.1016/j.jssc.2006.12.016

hafnium impurities tends to suppress the concentration of holes [14–17].

Interestingly, compare to Bi_2Te_3, Fe induces no ferromagnetism in Sb_2Te_3 and crystals of $Sb_{2-x}Fe_xTe_3$ ($x<0.02$) remain paramagnetic down to 2 K [18]. Measurements of the transport parameters and reflectance in the plasma resonance region show a clear increase in hole concentration due to incorporation of Fe in Sb_2Te_3 [19]. However, each Fe atom seems to donate about 0.5 hole. In this paper, we aim to elucidate this effect within a model of point defects.

2. Experimental

2.1. Growth of Fe-doped Sb_2Te_3 single crystals

The starting polycrystalline materials for growing the single crystals were prepared from Sb, Te elements of 5 N purity and from Fe_2Te_3.

The polycrystalline materials were prepared in conical quartz ampoules. The ampoules were charged with quantities of Sb, Te and Fe_2Te_3 in the ratio corresponding to the stoichiometry $Sb_{2-x}Fe_xTe_3$ ($x = 0.00$; 0.002; 0.005; 0.01; 0.02 and 0.06). The charged ampoules were then evacuated to a pressure of 10^{-3} Pa and sealed. The synthesis was carried out in a horizontal furnace at a temperature of 1073 K for 48 h.

The single crystals were grown using the Bridgman method. A conical quartz ampoule, containing the synthesized polycrystalline material, was placed in the upper warmer part of the Bridgman furnace, where it was annealed at 1003 K for 24 h. Then it was lowered into a temperature gradient of 400 K/5 cm at a rate of 1.3 mm/h.

This technique yielded single crystals 50 mm long, 10 mm in diameter, well cleavable, with their trigonal axis always perpendicular to the pulling axis. The orientation of the cleavage faces was carried out using the Laue method.

The actual concentration of Fe in samples for the reflectivity measurements was determined using atomic absorption spectrometry. The accuracy of the actual concentrations presented in Tables 1 and 2 was estimated to be 10%.

2.2. Reflectance measurements

Spectral dependences of the reflectance R in the plasma-resonance frequency region were measured at the room temperature in unpolarized light on natural (0001) cleavage faces using an FT-IR spectrometer Biorad FTS 45. The geometry of the experiment was such that the electric field vector **E** of the electromagnetic radiation was always perpendicular to the trigonal c-axis, i.e. $\mathbf{E}\perp\mathbf{c}$. Since the measured area of the samples was 2 mm in diameter an

Table 1
Optical parameters of Fe-doped Sb_2Te_3 single crystals obtained from reflectance measurements. ω_p is plasma resonance frequency, τ optical relaxation time, and P concentration of free holes

Sample no.	c_{Fe}[a] (10^{19} cm^{-3})	ω_p (10^{14} s^{-1})	τ (10^{-14} s)	P (10^{19} cm^{-3})	ΔP[b] (10^{19} cm^{-3})	$\Delta P/c_{Fe}$ (dimensionless)
1	0	1.88	2.4	6.71	0	—
2	5.24	2.19	1.6	9.10	2.39	0.46
3	7.01	2.24	1.4	9.53	2.83	0.40
4	7.44	2.33	1.2	9.94	3.23	0.43
5	7.79	2.35	1.0	10.22	3.51	0.45
6	8.29	2.36	1.1	10.10	3.39	0.41
7	9.14	2.4	1.1	10.49	3.79	0.41
8	9.49	2.37	1.1	10.40	3.70	0.39

[a]Estimated error of analysis $\pm 10\%$.
[b]$\Delta P = P - P_0$ (where P is hole concentration in the given sample and P_0 is the hole concentration in pure Sb_2Te_2).

Table 2
Concentration of the point defects and free carriers in Fe-doped Sb_2Te_3 crystals

Sample no.	c_{Fe}[a] (10^{19} cm^{-3})	ΔP (10^{19} cm^{-3})	$[Sb'_{Te}]$ (10^{19} cm^{-3})	$[{}^1Fe^{\times}_{Sb}]$ (10^{19} cm^{-3})	$[{}^2Fe^{\times}_{Sb}]$ (10^{19} cm^{-3})	$[V^{\bullet\bullet}_{Te}]$ (10^{19} cm^{-3})	$[Sb^{\times}_{Sb}]$ (10^{19} cm^{-3})	$[V^{\bullet\bullet}_{Te}]_{act}$ (10^{19} cm^{-3})
1	0.00	0.00	11.72	0.00	0.00	20.08	9.48	2.50
2	5.24	2.39	12.12	4.84	0.40	19.69	9.08	1.51
3	7.01	2.83	12.19	6.54	0.47	19.62	9.01	1.30
4	7.44	3.23	12.26	6.90	0.54	19.55	8.94	1.16
5	7.79	3.51	12.30	7.21	0.58	19.50	8.90	1.04
6	8.29	3.39	12.29	7.73	0.57	19.52	8.91	1.09
7	9.14	3.79	12.35	8.51	0.63	19.45	8.85	0.93
8	9.49	3.70	12.34	8.87	0.62	19.46	8.86	0.97

[a]Estimated error of analysis $\pm 10\%$.

influence of a possible concentration gradient can be excluded.

3. Experimental results

Results of reflectance measurements for several samples are depicted in Fig. 1. The reflectance curves $R=f(\nu)$ reveal distinct minima that evidence a good crystalline quality of the samples. With an increasing iron content in the samples this minimum is shifted towards higher wavenumbers. Simultaneously we can observe in Fig. 1, that the depth of the reflectance minimum decreases with an increasing iron content in the samples.

At this point, we have to note that the observed difference in the depth of the reflectance minima is not due to variations in the quality of the prepared crystals. The crystals of both "pure" Sb_2Te_3 as well as all iron-doped crystals were well cleavable and the perfect natural cleavage faces of all samples were mirror smooth.

In order to obtain information on the changes in the free-carrier concentration, associated with an incorporation of Fe into the Sb_2Te_3 lattice, the experimental $R=f(\nu)$ curves were fitted using equations for the real (ε_1) and imaginary (ε_2) parts of the permittivity [20]:

$$\varepsilon_1 = n^2 - k^2 = \varepsilon_\infty \left(1 - \frac{1}{(\omega/\omega_p)^2 + (1/\omega_p\tau)^2}\right), \quad (1)$$

$$\varepsilon_2 = 2nk = \frac{\varepsilon_\infty}{\omega\tau}\frac{1}{(\omega/\omega_p)^2 + (1/\omega_p\tau)^2}, \quad (2)$$

where n is the index of refraction, k index of extinction, τ the optical relaxation time, ε_∞ the high-frequency permittivity, and ω_p the plasma resonance frequency. For a single type of carriers, the last quantity is given by the relation

$$\omega_p = \left(\frac{Pe^2}{\varepsilon_0\varepsilon_\infty m_\perp m_0}\right)^{1/2}, \quad (3)$$

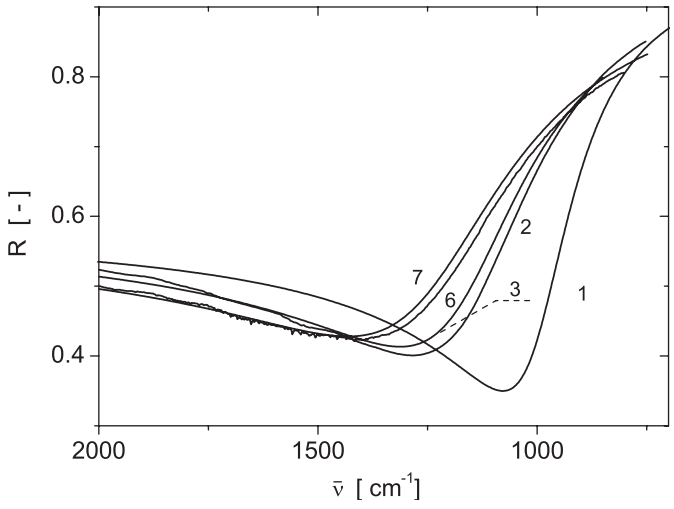

Fig. 1. Reflectance spectra of the Fe-doped Sb_2Te_3 single crystals. Samples are labeled according to Table 1.

where $m_\perp m_0$ is the carrier effective mass in the direction perpendicular to the trigonal axis c, P is the concentration of free carriers, and ε_0 is the permittivity of the free space.

Using the fitted values of ε_∞ and ω_p we determined, with the aid of Eq. (3), the values of the ratio $P/m_\perp$. Making a simplifying approximation that the value of $m_\perp$ is constant in the investigated interval of the carrier densities, the ratios $P/m_\perp$ were used to calculate the charge carrier concentrations P. In this calculation, we took the value of $m_\perp = 0.109m_o$, the value determined from $m_\parallel = 0.26m_o$ [21] and the ratio $m_\parallel/m_\perp = 2.36$ [22]. The results of this analysis are summarized in Table 1. It is evident that the values of P increase with the increasing content of iron. From the results, we figured out the ratio $\Delta P/c_{Fe}$ denoting the number of holes produced per one incorporated Fe atom. In the following discussion, we shall attempt to explain the fact, that one Fe atom in $Sb_{2-x}Fe_xTe_3$ produces only a fraction of a hole.

Note: according to the results presented in [23], for the Sb_2Te_3 crystals we should take into account a splitting of the valence band and, consequently, the presence of two types of holes—those the upper valence band (UVB) and those in the lower valence band (LVB). However, the ratio of the concentration of holes in the LVB to that in the UVB is equal to 390 [23]. Therefore, we assume that for the analysis of the reflectance spectra only the LVB-holes need to be considered.

4. Discussion

4.1. Point defects in $Sb_{2-x}Fe_xTe_3$ crystals

According to the last column in Table 1, it is evident that one Fe atom in the crystal structure of Sb_2Te_3 produces 0.4–0.5 hole. In following paragraphs, we attempt to explain this result. To do so, we first describe the native defects in the Sb_2Te_3 structure and how one determines their concentration. We then consider possible interactions between the incorporated Fe atoms and these native defects.

As is well known [24], crystals of Sb_2Te_3 prepared from stoichiometric mixtures of Sb and Te by the Bridgman method reveal an overstoichiometric amount of Sb atoms. These overstoichiometric atoms can form the following defects:

(a) Te vacancy $V_{Te}^{\bullet\bullet}$ carrying two positive charges, Sb vacancy V_{Sb}''' carrying three negative charges,
(b) antisite defects consisting of Sb atoms located on the Te sublattice that carry one negative charge, Sb_{Te}', (AS defects),
(c) structural defects of seven- or nine-layer lamellae Sb_3Te_4', Sb_4Te_5'' carrying one or two negative charges, respectively.

We cannot exclude the presence of more than one type of defects and, in fact, accept a simultaneous presence of defects such as ($V_{Te}^{\bullet\bullet}$ and Sb_{Te}') and ($V_{Te}^{\bullet\bullet}$ and Sb_3Te_4').

Furthermore, we adopt the following principles and simplifications:

- The native defects arise during the crystal growth, i.e., on transition from the melt to the solid phase.
- The formation of native defects approaches an equilibrium state, that can be formulated according to [25] by means of the equation

$$Sb_{Sb}^{\times} \Leftrightarrow Sb'_{Te} + (1+2/3)V'''_{Sb} + 6h^{\bullet}. \quad (4)$$

This equation (using relation $2V'''_{Sb} + 3V^{\bullet\bullet}_{Te} = 0$) determines equilibrium concentrations of defects and free carriers

$$Sb_{Sb}^{\times} + V^{\bullet\bullet}_{Te} + 2e' \Leftrightarrow Sb'_{Te} + V'''_{Sb} + 4h^{\bullet}, \quad (4a)$$

where $h^{\bullet}$ denotes a free hole, e′ a free electron, $Sb_{Sb}^{\times}$ denotes a Sb atom on a regular site.

To calculate the concentration of antisite defects Sb'_{Te} and the two types of vacancies V'''_{Sb} and $V^{\bullet\bullet}_{Te}$ we use a simple model based on the idea that only a certain part of the total overstoichiometric antimony content Sb_{over} is incorporated in the antimony sublattice (denoted $Sb_{Sb}^{\times}$), which gives rise to tellurium vacancies $V^{\bullet\bullet}_{Te}$. The remaining part enters the Te sublattice forming antisite defects Sb'_{Te}. According to Eq. (4a) the formation of one antisite defect Sb'_{Te} means formation of one vacancy V'''_{Sb}. The model respects the ratio of cation to anion sites equal to 2:3 and implies the following relations:

$$[Sb_{over}] = [Sb_{Sb}^{\times}] + [Sb'_{Te}],$$
$$2[V^{\bullet\bullet}_{Te}] + [h^{\bullet}] = [Sb'_{Te}],$$
$$[V'''_{Sb}] = [Sb'_{Te}],$$
$$([Sb_{Sb}^{\times}] + [V'''_{Sb}])/([V^{\bullet\bullet}_{Te}] + [Sb'_{Te}]) = 2/3. \quad (5a-d)$$

Square brackets denote concentration of the defects.

Chemical analysis gives the stoichiometry $Sb_2Te_{2.95}$, i.e., $Sb_{over} = 21.2 \times 10^{19}$ Sb-atom/cm^3. The hole concentration obtained from Hall measurements for this stoichiometry is $p = 6.71 \times 10^{19}\,cm^{-3}$.

Using the above equations and the results of chemical analysis obtained on this nonstoichiometric $Sb_{2+\delta}Te_3$, the concentrations of defects were determined as $[Sb'_{Te}] = 11.72 \times 10^{19}\,cm^{-3}$, $[Sb_{Sb}^{\times}] = 9.48 \times 10^{19}\,cm^{-3}$, $[V^{\bullet\bullet}_{Te}] = 20.08 \times 10^{19}\,cm^{-3}$, $[V'''_{Sb}] = 11.72 \times 10^{19}\,cm^{-3}$.

We note that with respect to the relation $2V'''_{Sb} + 3V^{\bullet\bullet}_{Te} = 0$ the concentration of electrically active vacancies $[V^{\bullet\bullet}_{Te}]_{act} = 2.50 \times 10^{19}\,cm^{-3}$.

The knowledge of the character and concentrations of native defects in nonstoichiometric $Sb_{2+\delta}Te_3$ allows us to explain the observed doping properties of Fe in Sb_2Te_3 crystal; Fe atoms entering the crystal structure interact with native defects. There are some limitations for the incorporation of Fe atoms into the crystal structure:

- Fe atoms cannot incorporate into anion sublattice.
- According to [18] all Fe atoms are in the oxidation state (+3).
- The formation of interstitial Fe^{+3} does not correspond to the increase in the hole concentration.

Under these conditions there are two possible mechanisms of the incorporation of Fe atoms into the Sb_2Te_3 crystal structure described by the following equations:

$$(2V'''_{Sb} + 3V^{\bullet\bullet}_{Te}) + 2Fe + 3Te = 2Fe_{Sb}^{\times} + 3Te_{Te}, \quad (6)$$

$$Sb_{Sb}^{\times} + V^{\bullet\bullet}_{Te} + 2e' + (Fe^{+3} + 3e') = Sb'_{Te} + Fe_{Sb}^{\times} + h^{\bullet}. \quad (7)$$

Eq. (6) describes the entering of Fe atoms in cation vacancies, which gives rise to uncharged substitutional defect $Fe_{Sb}^{\times}$. Eq. (7) describes the interaction of Fe atom (entering the structure) with overstoichiometric antimony $Sb_{Sb}^{\times}$ and vacancy $V^{\bullet\bullet}_{Te}$, which means shift of equilibrium towards formation of Sb'_{Te} and V'''_{Sb} point defects according to Eq. (4a). Equation implying the incorporation of Fe with addition of stoichiometric Te (2Fe+3Te) gives the same result

$$(2Sb_{Sb} + 3Te_{Te}) + (2Fe + 3Te) + 2(2V'''_{Sb} + 3V^{\bullet\bullet}_{Te}) = 2Sb'_{Te} + 2Fe_{Sb}^{\times} + 6Te_{Te} + 4V'''_{Sb} + V^{\bullet\bullet}_{Te} + 12h^{\bullet}. \quad (8)$$

Eqs. (6)–(8) comply with the above given conditions. The incorporation of Fe atoms into the cation sublattice (Eq. (6)) leads to the formation of the substitutional uncharged defects $Fe_{Sb}^{\times}$. Also, the incorporation of Fe according to Eq. (8), which results in the formation of covalently bonded of Fe atoms (in formal state +3) is in accord with the results of magnetic susceptibility measurements [18].

The proposed incorporation of Fe atoms into the crystal structure of Sb_2Te_3 as described by Eqs. (6) and (8) helps us to explain the observed doping properties of Fe atoms and the increase in the concentration of holes. We proceed by designating as ^{1}Fe a fraction of Fe atoms that enter the cation vacancies and form substitutional uncharged defects $Fe_{Sb}^{\times}$ in the process described by Eq. (6). Then, another fraction of Fe atoms, denoted as ^{2}Fe, shifts the equilibrium reaction (Eq. (4)) in favor of antisite defects, vacancies, and holes. Sb atoms from cation sublattice move on the anion sublattice where they form antisite defects Sb'_{Te}. This transition is accompanied by the formation of 4 holes (see Eq. (4)). The produced 4 holes together with the disappearance of one $V^{\bullet\bullet}_{Te}$ give rise to an overall shift by 6 holes. Thus, the ^{1}Fe-atoms do not affect the concentration of holes while the ^{2}Fe atoms liberate 6 holes. This consideration results in several simple relations:

$$[^1Fe] + [^2Fe] = c_{Fe}, \quad P_1(^1Fe_{Sb}^{\times}) + P_2(^2Fe_{Sb}^{\times}) = \Delta P \quad (9a)$$

because

$$P_1(^1Fe_{Sb}^{\times}) = 0, \quad P_2(^2Fe_{Sb}^{\times}) = 6[^2Fe_{Sb}^{\times}]. \quad (9b)$$

From Eqs. (9a) and (9b) we can estimate the concentrations of $[^1Fe_{Sb}^{\times}]$ and $[^2Fe_{Sb}^{\times}]$, while from Eq. (8) we can obtain the concentration of $V^{\bullet\bullet}_{Te}$, Sb'_{Te}, $Sb_{Sb}^{\times}$ and V'''_{Sb}, and the concentration of active Te-vacancies $[V^{\bullet\bullet}_{Te}]_{act}$. The resulting data provide the information on interactions, i.e., we obtain the concentration of holes created by the

incorporation of ^{2}Fe atoms, changes in the concentration of antisite defects, the concentration of $[V_{Te}^{\bullet\bullet}]$, and the concentration of $[^2Fe_{Sb}^{\times}]$. These results are given in Table 2. The changes in the concentration of all the defects with the concentration of incorporated Fe are given in Fig. 2.

The results presented in Table 2 show also that the changes in the hole concentration associated with the incorporation of Fe into the Sb_2Te_3 structure are due to an increase in the concentration of $(Sb_{Te}' + V_{Sb}''')$ and a concomitant suppression in the concentration of $V_{Te}^{\bullet\bullet}$ and $Sb_{Sb}^{\times}$.

4.2. Free-carrier scattering mechanism in $Sb_{2-x}Fe_xTe_3$ crystals

As the measurements of the reflectance spectra of the Fe-doped Sb_2Te_3 crystals showed, with the increasing content of Fe not only the plasma-resonance frequency changes, but also the character of the spectral dependence $R(\nu)$ changes; i.e., the reflectance minimum is not so deep, which indicates a change in the optical relaxation time τ (see Table 1). Thus, it would be reasonable to examine possible changes in the mechanism of the scattering of free current carriers with compositional changes. The changes in the scattering mechanism can be evaluated from the analysis of the dielectric function ε_2. Using Eq. (2) we have obtained the spectral dependence of the imaginary part of the dielectric function ε_2 (ν) in the considered frequency range. In the case of narrow-gap semiconductors the imaginary part ε_2 is generally given by the equation

$$\varepsilon_2(\nu) = \varepsilon_2^{FC}(\nu) + \varepsilon_2^{IB}(\nu), \tag{10}$$

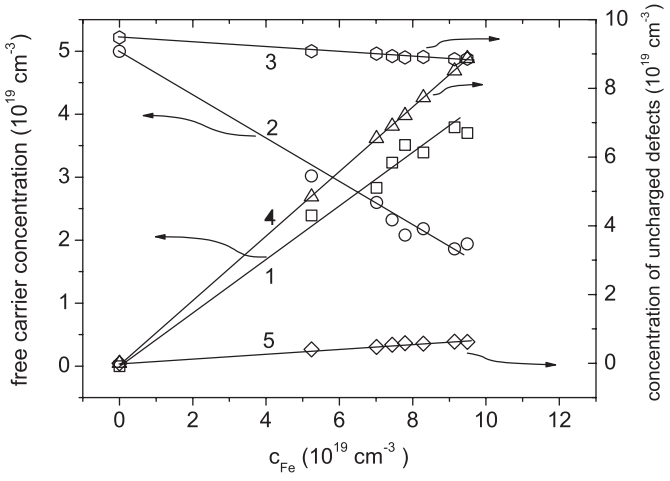

Fig. 2. Model of defects in Fe-doped Sb_2Te_3 crystals. Curve #1: Increase in the concentration of holes ΔP caused by the incorporation of Fe atoms in the lattice, curve #2: concentration of electrons produced by Te vacancies $[V_{Te}^{\bullet\bullet}]_{act}$, curve #3: concentration of overstoichiometric antimony content incorporated in the antimony sublattice $[Sb_{Sb}^{\times}]$, curve #4: concentration of Fe atoms incorporated in the crystal according to the Eq. (6) $[^1Fe_{Sb}^{\times}]$, curve #5: concentration of Fe atoms incorporated in the crystal according to the Eq. (7) $[^2Fe_{Sb}^{\times}]$.

where $\varepsilon_2^{FC}(\nu)$ is associated with free charge carriers and $\varepsilon_2^{IB}(\nu)$ is associated with interband transitions [26]. In case of the crystals studied in this paper no contribution of interband transition ($E_g \approx 0.2$ eV) is observed in the vicinity of plasma resonance frequency (see Fig. 1) and $\varepsilon_2^{IB}(\nu)$ is not further considered. According to the [27] paper following expression holds:

$$\varepsilon_2^{FC}(\nu) \sim (\nu)^{-\kappa}. \tag{11}$$

In the quantum-mechanical limit ($hc\nu > 2k_BT$; h is the Planck constant, c is the velocity of light, k_B is the Boltzmann constant, T is the absolute temperature) the exponent κ depends on the mechanism of free-carrier scattering. For the nondegenerate free-carrier gas the scattering on acoustic phonons takes place and the exponent $\kappa = 2.5$, for polar optical and piezoelectric scattering $\kappa = 3.5$, and for scattering on ionized impurities $\kappa = 4.5$.

Even though Eq. (11) was derived for the nondegenerate free carriers, it was shown [28] that it can be applied also for a partially degenerate free-carrier system.

From the log-log dependence of ε_2 versus ν (Fig. 3), we obtained the same value of the exponent $\kappa \sim 2.7$ for both undoped Sb_2Te_3 and Fe-doped samples. This value suggests that free-carrier scattering is dominated by acoustic phonons ($\kappa_{ap} \sim 2.5$) with a small contribution coming from scattering on ionized impurities. The contribution of polar optical scattering at room temperature can be excluded since the Sb_2Te_3 crystals belong to the space group of D_{3d}^5. This conclusion is supported by the results of the study concerning the scattering mechanism of free carriers in the isostructural Bi_2Se_3 crystal [28,29], where the mixed scattering mechanism on acoustic phonons and ionized impurities was confirmed.

The results of measurements of Hall effect and electrical conductivity [18] also suggest a mixed scattering mechanism on acoustic phonons and ionized impurities. As is well known, the exponent k in the relation $R_H\sigma \sim T^{-k}$

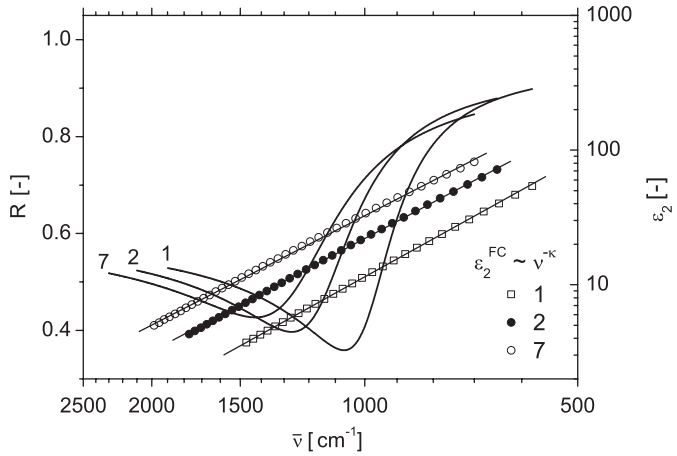

Fig. 3. Logarithmic dependence ε_2^{FC} vs. $\bar{\nu}$ (symbols) with linear fits (dashed lines) in the plasma resonance frequency region and reflectance spectra (solid lines) of Fe-doped Sb_2Te_3 crystals. Samples are labeled according to Table 1.

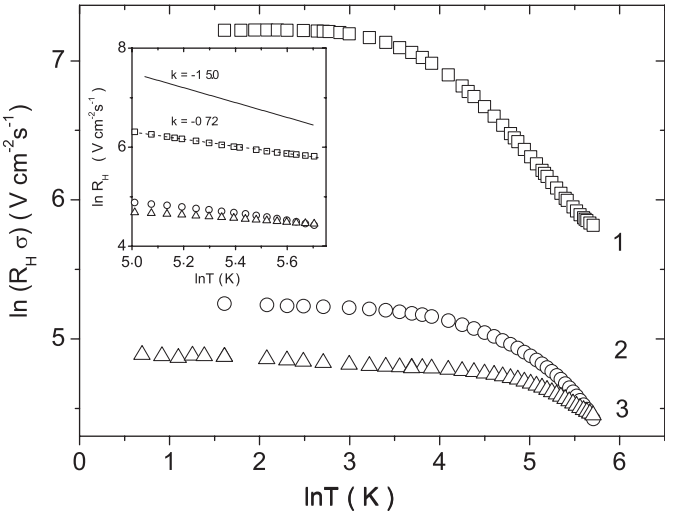

Fig. 4. Logarithmic dependence of Hall mobility for Fe-doped Sb_2Te_3 crystals: curve #1: undoped Sb_2Te_3, curve #2: $c_{Fe} = 5.25 \times 10^{19}\,cm^{-3}$, curve #3: $c_{Fe} = 1.12 \times 10^{19}\,cm^{-3}$. In the inset are compared the exponents k in the relation $R_H\sigma \sim T^{-k}$ with $k = -3/2$ (solid line), the value that corresponds to scattering on acoustic phonons.

characterizes the scattering mechanism. With the aim of examining the scattering mechanism governing transport properties we plot $\ln(R_H\sigma) = f(\ln T)$ in Fig. 4. In the inset of Fig. 4 we compare the slopes of $\ln(R_H\sigma) = f(\ln T)$ with the line of slope $-3/2$ that corresponds to scattering on acoustic phonons. Absolute values of the slopes of all samples are smaller than $-3/2$ which suggests that the mixed scattering mechanism is at play. From Fig. 4, it is evident that the contribution due to ionized impurity scattering increases with the decreasing temperature.

Both the transport (Fig. 4) and optical measurements (relaxation time τ in Table 1) show that the incorporation of Fe results in a decrease in free-carrier mobility.

5. Conclusions

(a) Single crystals of $Sb_{2-x}Fe_xTe_3$ ($c_{Fe} = 0$–$9.5 \times 10^{19}\,cm^{-3}$) were characterized by measurements of reflectance spectra in the plasma resonance frequency region. Plasma frequency ω_P ($\mathbf{E} \perp c$) was used for the determination of free-carrier concentration. We have found that one incorporated Fe atom liberates 0.4–0.5 hole.

(b) Doping properties of Fe atoms were elucidated using a model of interaction of Fe atoms entering the crystal lattice with native defects—AS defects, V'''_{Sb} vacancies and $V^{\bullet\bullet}_{Te}$ vacancies. The model is characterized by two simultaneous reactions:
   (1) A fraction of Fe atoms enters cation vacancies and forms substitutional uncharged defects $Fe^{\times}_{Sb}$. This reaction does not change the free-carrier concentration.
   (2) The remaining fraction of Fe atoms enters the cation sublattice giving rise to both the antisite defects Sb'_{Te} and undoped substitution defects $Fe^{\times}_{Sb}$. According to the above proposed model, this interaction is accompanied by an increase in the concentration of holes and a suppression in the concentration of $V^{\bullet\bullet}_{Te}$.

(c) Entering Fe atoms do not affect the scattering mechanism of free carriers. The scattering on acoustic phonons is dominant in both undoped Sb_2Te_3 and doped $Sb_{2-x}Fe_xTe_3$ crystals in the vicinity of 300 K.

Acknowledgments

The research was supported by Ministry of Education, Youth and Sports of the Czech Republic under the project MSM 0021627501 and by the grants NSF-INT 0201114 and NSF DMR-0305221.

References

[1] H. Krebs, Grundzüge der Anorganishen Kristallchemie, F. Enke-Verlag, Stuttgart, 1968, p. 239.
[2] H.J. Goldsmid, Thermoelectric Refrigeration, Plenum Press, New York, 1964, p. 113.
[3] V.A. Kulbachinskii, A.Yu. Kaminskii, K. Kindo, Y. Narumi, K. Suga, P. Lošťák, P. Švanda, JETP Lett. 73 (2001) 352.
[4] V.A. Kulbachinskii, A.Yu. Kaminskii, K. Kindo, Y. Narumi, K. Suga, P. Lošťák, P. Švanda, Phys. Lett. A 285 (2001) 173.
[5] J.S. Dyck, W. Chen, P. Hájek, P. Lošťák, C. Uher, Physica B 312–313 (2002) 820.
[6] J.S. Dyck, P. Hájek, P. Lošťák, C. Uher, Phys. Rev. B 65 (2002) 115212.
[7] Z. Zhou, Y.-J. Chin, C. Uher., Appl. Phys. Lett. 87 (2005) 112503.
[8] P. Lošťák, Č. Drašar, J. Navrátil, L. Beneš, Cryst. Res. Technol. 31 (1999) 403.
[9] J.S. Dyck, Č. Drašar, P. Lošťák, C. Uher, Phys. Rev. B 71 (2005) 115214.
[10] V.A. Kulbachinskii, P.M. Tarasov, E. Brück, JETP 101 (2005) 528.
[11] V.A. Kulbachinskii, P.M. Tarasov, E. Brück, Physica B 368 (2005) 32.
[12] J.S. Dyck, P. Švanda, P. Lošťák, J. Horák, W. Chen, C. Uher, J. Appl. Phys. 94 (2003) 7631.
[13] J. Horák, P. Lošťák, Č. Drašar, J.S. Dyck, Z. Zhou, C. Uher, J. Solid State Chem. 178 (2005) 2907.
[14] Č. Drašar, P. Lošťák, J. Navrátil, T. Černohorský, V. Mach, Phys. Status Solidi B 191 (1995) 523.
[15] Č. Drašar, M. Steinhart, P. Lošťák, H.-K. Shim, J.S. Dyck, C. Uher, J. Solid State Chem. 178 (2005) 1301.
[16] P. Lošťák, Č. Drašar, I. Klichová, J. Navrátil, M. Vlček, Cryst. Res. Technol. 32 (1997) 369.
[17] T. Plecháček, J. Navrátil, P. Hájek, A. Krejčová, P. Lošťák, in: Proceedings of XII International Conference on Thermoelectrics, La Grande Motte, August 2003, p. 38.
[18] Z. Zhou, M. Žabčík, P. Lošťák, C. Uher, J. Appl. Phys. 99 (2006) 043901.
[19] P. Švanda, P. Lošťák, Č. Drašar, J. Navrátil, L. Beneš, T. Černohorský, Radiat. Effects Defects Solids 153 (2000) 59.
[20] O. Madelung, in: S. Flügge (Ed.), Handbuch der Physik Bd. XX, Springer, Berlin, 1957, p. 210.
[21] W. Richter, A. Krost, V. Nowak, E. Anastassakis, Z. Phys. B 49 (1982) 191.
[22] J. Horák, P. Lošťák, L. Šiška, M. Stordeur, Phys. Status Solidi B 114 (1982) 39.
[23] V.A. Kulbachinskii, Z.M. Dashevskii, M. Inoue, M. Sasaki, H. Negishi, W.X. Gao, P. Lošťák, J. Horák, A. de Visser, Phys. Rev. B 52 (1995) 10915.
[24] G. Offergeld, J. van Cakenberghe, J. Phys. Chem. Solids 11 (1959) 310.

[25] F.A. Kroeger, The Chemistry of Imperfect Crystals, vol. 2, North-Holland, Amsterdam, Oxford, New York, 1974, p. 244.
[26] E. Gerlach, P. Grosse, Festkörperprobleme 17 (1977) 157.
[27] M. Stölzer, M. Stordeur, H. Sobotta, V. Riede, Phys. Status Solidi B 138 (1986) 259.
[28] M. Stordeur, K.K. Ketavong, A. Priemuth, H. Sobotta, V. Riede, Phys. Status Solidi B 169 (1992) 505.
[29] J. Navrátil, T. Plecháček, J. Horák, S. Karamazov, P. Lošťák, J.S. Dyck, W. Chen, C. Uher, J. Solid State Chem. 160 (2001) 474.